Incorporation of Ge in ferrihydrite: Implications for the structure of ferrihydrite

(4312-Revision 3)

DOGAN PAKTUNC[1,2]*, **ALAIN MANCEAU**[3] and **JOHN DUTRIZAC**[1]

[1]CanmetMINING, 555 Booth St., Ottawa, ON, K1A 0G1, Canada

[2]Department of Earth Sciences, University of Ottawa, Ottawa, ON, K1N 6N5, Canada

[3]ISTerre-Maison des Géosciences, CNRS and Université J. Fourier, BP 53, 38041 Grenoble, France

*corresponding author: *dpaktunc@NRCan.gc.ca*

ABSTRACT

Germanium-bearing ferrihydrites containing 0.2, 0.6, 1.4, 2.2, 2.9, 3.8, 12 and 15 wt% Ge were synthesized in the laboratory at 25 and 65 ºC. X-ray diffraction analyses showed all the precipitates to be six-line ferrihydrite. Semi-quantitative energy-dispersive X-ray microanalyses (TEM) indicate that the precipitates made from solutions having Fe/Ge molar ratios of two and four have Fe/Ge atomic ratios of 3.9 and 4.8, respectively, which suggest a limit of Ge uptake in ferrihydrite of about 20 at% relative to total cations. Based on TEM examinations, these high Ge-bearing ferrihydrites are homogenous and consist of equant and plate-like crystallites about 5-6 nm in size. Furthermore, it appears that higher Ge concentrations have no significant effect on the crystallite size, supporting the incorporation of Ge in the ferrihydrite structure. Extended X-ray absorption fine structure (EXAFS) spectroscopy indicated that the Fe atoms in both the low and high Ge-bearing ferrihydrites are in octahedral coordination and that Ge occurs in the ferrihydrite structure by filling the empty tetrahedral sites and coordinating to 4 edge-sharing FeO_6 trimers through sharing a common oxygen (Ge-O-Fe linkage). Incorporation of the Ge tetrahedra in the ferrihydrite structure requires redistribution of Fe occupancy along the alternating O/OH layers while forming an ordered distribution of octahedral Fe and tetrahedral Ge. The local structure around Ge mimics a Keggin-like motif in two different, yet equivalent, orientations. It appears that the split diffraction peak at 1.46 and 1.51 Å is a characteristic feature of Ge-rich ferrihydrite and suggests that it is a fingerprint of increased order due to significant Ge incorporation in the tetrahedral sites. The findings can be rationalized in terms of the incorporation of Ge in the so-called "f-phase" of the classical ferrihydrite model, and demonstrate the flexibility of the model in terms of accommodating a Keggin-like cluster without the need of imposing unrealistic constraints as in the akdalaite model. Direct comparison of the imaginary parts of the Fourier transforms for ferrihydrite and maghemite further confirms the absence of tetrahedral Fe in ferrihydrite.

Keywords: Ferrihydrite, structure, germanium, iron, tetrahedral iron, EXAFS.

INTRODUCTION

Ferrihydrite is a poorly crystalline and metastable nano-sized ferric oxyhydroxide. It is widespread in soils, iron-rich oxidized sediments, acid mine drainage settings, mine wastes and Fe-rich hydrometallurgical process waters (Jambor and Dutrizac 1998). Because of its small size (i.e., 2-3.5 nm Eggleton and Fitzpatrick 1988; 1-6 nm Janney et al. 2000), its abundance, and the geochemical reactivity of the contained ferric ion, ferrihydrite plays an important role in iron cycling and in controlling nutrient and toxic element mobility and bioavailability in the near-surface environment.

Ferrihydrite has long been considered to be a mixture of defective and defect-free varieties, the so-called "d-phase" and "f-phase" (Drits et al. 1993a; Marchand and Rancourt 2009; Manceau 2009, 2011). More recently, Michel et al. (2007, 2010) proposed a new structural model for ferrihydrite which is single-phase, has a low density of defects, and is isostructural with the mineral akdalaite ($Al_{10}O_{14}(OH)_2$). Unlike the conventional model (Drits et al. 1993a; Manceau 2011), 20% of the Fe atoms are in tetrahedral coordination in the new model, and octahedra share corners and edges only, without a face-sharing arrangement. The new model received criticism because of its shortcomings in adequately describing the X-ray diffraction, X-ray absorption spectroscopy and Mössbauer data, and not being in accordance with fundamental crystal chemical principles (Rancourt and Meunier 2008; Hiemstra and van Riemsdijk 2009; Manceau 2009, 2010, 2011, 2012a).

Recently Song et al. (2010) reported incorporation of Ge in the ferrihydrite structure. In their synthesis experiments using dilute solutions, Ge was coprecipitated with Fe at a Fe/Ge molar ratio of 2 and pH 2, 5, 10 and 13, followed by aging at 95°C for 5 days. The final products were characterized by a combination of techniques and the authors interpreted the results as being supportive of the new structural model of Michel et al. (2007, 2010).

More than a decade ago, we synthesized Ge-bearing ferrihydrite from ferric sulfate and germanium tetrachloride solutions. The motivation was to test the ability and capacity of ferrihydrite to control impurities such as Ge in Fe-rich hydrometallurgical solutions. In the metallurgical industry, Ge is commonly concentrated from process solutions by ferrihydrite precipitation. Germanium-bearing ferrihydrite is later dissolved

in acid media and is further upgraded to produce a germanium product. In order to test the incorporation of Ge in the ferrihydrite structure as a surrogate of the tetrahedrally-coordinated Fe(III) and to provide further insights to the ferrihydrite structural models, we reanalysed our old samples and performed additional synthesis experiments using a protocol similar to that of Song et al. (2010) but much expanded in terms of solution compositions and synthesis temperatures. In this contribution, we report our findings on the nature of Ge coprecipitated with Fe under conditions promoting the formation of six-line ferrihydrite.

METHODOLOGY

Our earlier synthesis experiments were performed at 65 °C from 0.1 M $Fe(SO_4)_{1.5}$ and dilute $GeCl_4$ solutions at pH 2.5 to 3.2. Germanium concentrations in the starting solutions were 0.2, 0.5, 1.0, 1.4, 1.9 and 2.4 mM with corresponding Fe/Ge molar ratios of 435, 213, 105, 71, 54 and 43. The solution pH was adjusted to the desired value by the slow addition of 0.3 M NaOH at 4.8 mL/min. The final products were filtered and washed with deionized water. The extent of Ge precipitation ranged from 63 to 89%, corresponding to solutions with Fe/Ge molar ratios that ranged from 43 to 435 and final products ranging from 3.8 to 0.2% Ge.

Our more recent synthesis experiments followed a protocol similar to that reported by Song et al. (2010). The experiments were performed at room temperature using solutions containing 0.002 M $Fe(NO_3)_3{\cdot}9H_2O$ and 0.001 M Ge(IV) ethoxide ($GeO_4(C_2O_5)_4$) at pH 2, 5, 10 and 13. The ferric nitrate solution in the reactor was continuously stirred at high speed during the drop-wise addition of Ge(IV) ethoxide. The solution pH was subsequently adjusted to 2, 5, 10 and 13 by the addition of 1 M NaOH at a rate of 0.5 mL/min, and then the solution pH was rapidly decreased to about 1.5 by adding 20% HNO_3. The resulting slurries were stirred for an additional hour at room temperature before they were aged in an oven at 95 °C for 5 days. The products were centrifuged, washed several times with dionized water and ethanol, dialyzed, and freeze dried. The synthesis experiments were performed at a Fe/Ge molar ratio of two as in Song et al. (2010), and also at four to test the effect of Ge concentration in the starting

solution. As a control, synthesis experiments were also performed at pH 2 without the addition of Ge following the same protocol.

X-ray diffraction analyses were performed by a Rigaku D/MAX 2500 rotating anode X-ray powder diffractometer using CuKα radiation at 50 kV and 260 mA with a step size of 0.02° and scan rate of 1°/min in 2θ. The samples were placed on zero-background plates and disseminated by acetone for the X-ray powder diffraction analysis. For monitoring purposes and very small samples in capillary tubes and small zero-background holders, a rotating anode Rigaku Rapid-2-R micro-XRD with a curved image plate was also used.

Extended X-ray absorption fine structure (EXAFS) spectroscopy measurements were made at the PNC-CAT bending magnet beamline of the Advanced Photon Source. The samples were prepared separately for Fe K-edge and Ge K-edge EXAFS by diluting with boron nitride and homogenizing to achieve a sample thickness of 1 absorption length. The monochromator crystals were detuned to 20% to eliminate harmonic contributions. The EXAFS spectra were collected at room temperature in both the transmission and fluorescence modes. Only the transmission measurements were used in the analysis with the exception of the Ge K-edge EXAFS spectra of the dilute Ge precipitates. Each sample was analysed 10 to 12 times and the spectra were averaged. Data reduction and analysis were accomplished by ATHENA and IFFEFIT/ARTEMIS (Ravel and Newville, 2005).

TEM samples were prepared from nine samples, listed on Table 1, by placing a drop of the dilute precipitate in solution after ultrasonication in ethanol onto a Lacey Carbon Film on a copper TEM grid. TEM examination was performed using a JEOL 2010 STEM operated at 200 kV. Semi-quantitative Fe and Ge microanalyses were performed using a Link (Oxford) PentaFET energy dispersive X-ray spectrometer.

RESULTS

X-Ray Diffraction

XRD patterns of the precipitates indicate that they are six-line ferrihydrite (Fig.1). The peaks of the samples synthesized from solutions with Fe/Ge molar ratios of 2 and 4 are at 2.525, 2.232, 1.972, 1,721, 1.509 and 1.461 Å, coinciding with the *d*-spacing values

of the Ge-bearing ferrihydrite reported by Song et al. (2010) and corresponding to six-line ferrihydrite (e.g., Childs et al. 1982; Eggleton and Fitzpatrick 1988; Drits et al. 1993a). Two characteristic features of these Ge-bearing ferrihydrites are the hump at about 2.50 Å from the 101 reflection, and the presence of the split peak at 1.51 and 1.46 Å from the 105 and 110 reflections. Better resolution of these peaks indicates that the Ge-bearing ferrihydrite crystals have a higher crystallinity in the c direction and *ab* plane. The split peak is a characteristic feature of the Ge-ferrihydrite and suggests that it is a fingerprint of increased order due to Ge incorporation. Germanium-bearing ferrihydrites synthesized at higher Fe/Ge molar ratios (i.e., ratios ≥43) do not display the split peak and they appear to be less ordered. The split peak at 1.51 Å is not detected in many of the XRD patterns reported for six-line ferrihydrite. A subtle peak at the *d*-spacing value of 4.2 Å (2θ=21.1°) indicates the presence of minor goethite in some of the samples (Fig. 1).

The precipitates formed from solutions without Ge (i.e., control experiments) yielded goethite and hematite indicating that the presence of Ge stabilized ferrihydrite preventing its transformation to hematite and goethite.

Transmission Electron Microscopy

The synthesis products formed at pH 2, 5, 10 and 13 from solutions with Fe/Ge molar ratios of 2 and 4 were characterized by TEM. All the synthesis products are homogenous and consist of equant and plate-like crystallites. They often display faceted hexagonal outlines with sub rounded corners (Fig. 2). Crystallite sizes of the precipitates are relatively uniform at 5.2 ± 1.0 nm and 6.2 ± 1.6 nm for pH 2, 5.5 ± 1.0 and 5.7 ± 1.2 nm for pH 5, 5.6 ± 1.1 nm and 6.0 ± 1.5 nm for pH 10, and 6.2 ± 1.6 and 6.2 ± 1.7 nm for pH 13 for precipitates having Fe/Ge molar ratios of 2 and 4, respectively. The data presented in Table 1 suggest little pH or compositional control on the crystallite sizes. This conclusion is different than the findings of Song et al. (2010) for Ge-bearing ferrihydrites precipitated from solutions with Fe/Ge molar ratios of 2 (i.e., 10 nm for pH 13 and 40 nm for pH 5). Our crystallite sizes are comparable to the reported size ranges for Ge-free six-line ferrihydrite (e.g., 5-10 nm by Childs et al. 1982; 4-5 nm by Saleh and Jones 1984; 4-5 nm by Eggleton and Fitzpatrick 1988; 5-6 nm by Janney et al. 2000).

Furthermore, Dyer et al. (2010) reported crystallite sizes of less than 10 nm for Si-bearing ferrihydrite.

The size variation is small for the particles formed from solutions with higher Ge concentrations; that is, higher Ge concentrations in the solution have a negligible effect on the crystallite size. This suggests that the excess Ge in solution is controlling the particle growth by occupying the surface sites of the Fe oligomers during hydrolysis.

Selected area electron diffraction (SAED) patterns display 2 to 5 diffuse rings with uniform *d*-spacings averaging at 2.57, 2.26, 1.98, 1.74 and 1.50 Å for the samples with Fe/Ge molar ratios of 2 and 4. The average values are based on 22 SAED patterns. These values are comparable to the more precise *d*-spacings obtained from the powder XRD patterns. High-resolution TEM (HRTEM) images display well-developed lattice fringes with two to three sets of lattice fringes (Fig. 3).

Semi-quantitative energy-dispersive X-ray microanalyses of Fe and Ge indicate that the synthesis products have Fe/Ge atomic ratios in the 3.8 to 3.9 range for the Fe/Ge=2 precipitates and in the 4.4 to 5.1 range for the Fe/Ge=4 samples. It appears that the amount of Ge in the precipitate is limited to about 20 at% of the total cations (Fe+Ge) for the Fe/Ge=2 precipitates and to 17 at% of the total cations for the Fe/Ge=4 precipitates. In other words, the precipitation efficiency of Ge (i.e., the percentage of the initial Ge precipitated with ferrihydrite) was between 79 and 91% for the Fe/Ge=4 experiments, but only 51-53% for the Fe/Ge=2 tests. This would indicate a limit of Ge uptake of about 20 at% Ge at the cation sites in ferrihydrite. Because the ferrihydrite precipitates typically contain ~45 wt% Fe, the products can incorporate up to ~15 wt% Ge in their structure.

X-Ray Absorption Spectroscopy

The Ge K-edge position remained unchanged with pH and solution composition. The XANES spectra and post edge features are similar to the tetrahedrally-coordinated quartz polymorph of GeO_2 rather than the octahedrally-coordinated rutile-like GeO_2 (Bull et al. 2004).

Ge K-edge EXAFS spectra of the precipitates formed at different pH values for Fe/Ge molar ratios of 2 and 4 are identical (Fig. 4) indicating that the local structural environments around the Ge atoms are not influenced by pH. Accordingly, for use in

EXAFS fitting and further comparisons, the spectra were averaged to obtain one spectrum for each solution composition (i.e., r2 and r4). The spectra of the precipitates formed from solutions with Fe/Ge molar ratios of 43 and 54 are broadly similar although noisy above the *k* value of about 11 $Å^{-1}$. These spectra were also averaged to obtain one spectrum representing the dilute samples (r43+). As illustrated in Figure 5, the Ge-dilute average spectrum displays close similarities to the two Ge-concentrated average spectra, and this suggests that solution composition has little, if any, influence on the local structure of Ge. The spectra are different than those reported by Pokrovsky et al. (2006) for GeO_4 adsorbed onto goethite, suggesting differences in the local coordination environments of the different samples. Pokrovsky et al. (2006) also reported two co-precipitate samples showing some similarity in Fourier Transforms to our samples, but their corresponding EXAFS spectra were not available and their long-range identities were shown as "undetermined".

Our EXAFS fitting strategy involved fitting the first peak in the radial distribution function (RDF) in the $R + \Delta R$ -range from 1 to 2 Å (values uncorrected for phase-shift) followed by the sequential addition of Ge and/or Fe shells to simulate the first and second RDF peaks. EXAFS fitting resulted with coordination numbers of 4.8 ± 0.4 for the first shell of oxygen atoms at distances of 1.76-1.77 Å indicating that the Ge atoms are tetrahedrally coordinated to oxygen atoms (Table 2). These values are identical within precision to the Ge-O distances of 1.764 Å reported by Song et al. (2010) for Ge-Fe co-precipitated six-line ferrihydrite, 1.76 ± 0.01 Å in GeO_4 tetrahedra adsorbed onto goethite and a co-precipitate (Pokrovsky et al. 2006), and 1.76 ± 0.01 Å in synthetic talc (Martin et al. 1996). Other Ge-O distances based on tetrahedral crystal structures include 1.772 Å in brunogeierite, a Fe_2GeO_4 spinel (Welch et al. 2001), 1.76 ± 0.04 Å in a diopside-like structure (Hattori et al. 2000), 1.77 ± 0.04 Å in $Fe_3Ge_2O_8$ (Kato et al. 1983a), and 1.76 ± 0.02 Å in $Fe_{15}Ge_8O_{36}$ (Kato et al. 1983b). Calculated Ge-O distances from the first-principles density functional theory include 1.77-1.81 Å for GeO_4 tetrahedra adsorbed onto FeO_6 octahedra as bidentate corner-sharing surface complexes (Li et al. 2010). Other Ge-O distances include somewhat shorter values at 1.73 ± 0.03 Å (Price et al. 1998), 1.74 Å (Lu et al. 1985), 1.73 and 1.74 Å (Drewitt et al. 2010) and 1.72-1.74 Å (Micoulaut et al. 2006a and 2006b) in Ge-oxide glasses.

The second shell fitting considered four possible structural occurrences of GeO_4 tetrahedra in natural and synthetic materials: (1) as framework tetrahedra, (2) as tetrahedral sheets (double-chains or rings), (3) as single chains of tetrahedra including very short chains such as dimers and (4) as isolated tetrahedra. The first three models involve Ge-O-Ge linkages. In the first case for framework tetrahedra, there are four Ge atoms around a central Ge at a distance of 3.16-3.32 Å, as observed in the GeO_2 glass structure where GeO_4 tetrahedra are connected through corner oxygens and no-edge sharing tetrahedra exist (Lu et al. 1985; Price et al. 1998; Micoulaut et al. 2006a,b). In the second case, GeO_4 tetrahedra form layers through corner-linkages, resulting in Ge-Ge distances of 3.13-3.18 Å and Ge coordination numbers of 2-3, as observed in synthetic talc (Martin et al. 1996). In the third model, there are two Ge atoms around a central Ge at a distance of 3.10 Å, observed in the high-P clinopyroxene ($FeGeO_3$) structure of Hattori et al. (2000) or one Ge at 3.09 Å as in $Fe_3Ge_2O_8$ and $Fe_{15}Ge_8O_{36}$ (Kato et al. 1983a,b).

Simulations involving Ge as the second shell to test the presence of Ge-O-Ge linkages in the precipitate formed from a solution with the highest Ge (i.e., r2 or molar Fe/Ge=2) resulted in a Ge-Ge distance of 3.27 ± 0.02 Å for 4 Ge. This fit required a third shell of 4.4 Fe atoms at 3.42 ± 0.02 Å with the corresponding fitting parameters of the first shell of 4.8 ± 0.4 O at 1.76 Å. The Ge-Ge distance is too long in comparison with the Ge-Ge distances reported for dimers (3.09 Å), single chains (3.10 Å) and sheets (3.13 and 3.18 Å) but it is within the limit of the range of GeO_2 glasses. However, the second cation shell parameters (i.e., 4.4 Fe atoms at 3.42 ± 0.02 Å) are incompatible with an infinite framework of corner-linked GeO_4 tetrahedra. The other possibility of small clusters of corner-linked GeO_4 tetrahedra attached to ferrihydrite is also unlikely because it would require Ge coordination numbers of 2 and smaller. Furthermore, simulation of the dilute sample where the likelihood of a Ge-O-Ge linkage is very low resulted in Ge-Ge distances that are similar to those of the concentrated samples. In support of the TEM observations that the precipitates are composed of uniform ferrihydrite crystallites, the EXAFS data suggest that there are no Ge-O-Ge linkages in the precipitates and that the GeO_4 tetrahedra are isolated and attached to Fe octahedra as in the fourth structural model which can be represented by brunogeierite, a Fe_2GeO_4 spinel (Welch et al. 2001).

Our next set of simulations of the Ge K-edge spectra involved Fe as the second shell and Ge or Fe as the third shell of atoms. The position of the second RDF peak was reproduced for both the Fe+Fe and Fe+Ge models; however, the qualities of the fits were not adequate. Contribution of the multiple scattering paths, as in AsO_4 tetrahedra, was tested by sequentially adding the Ge-O1-O2, Ge-O1-Ge-O2, Ge-O1-Ge-O1 and Ge-O-Fe paths derived from FEFF calculations (Ankudinov et al. 1998) based on the crystal structures of Hattori et al. (2000) and Welch et al. (2001). These multiple scattering paths are labelled MS21 (Ge-O1-O2), MS31 (Ge-O1-Ge-O2), MS32 (Ge-O1-Ge-O1) and MS22 (Ge-O-Fe) following the designations of Manceau et al. (2007). The quality of the fit improved with the inclusion of MS21 and reproduced both the shape and magnitude of the second RDF peak. As listed on Table 2, there are about 6 and 2 Fe atoms at distances of 3.38 ± 0.03 and 3.54 ± 0.08 Å. Floating both Fe shells during the fit resulted in large uncertainties (e.g. 7.8±11.6 Fe at 3.38±0.03 Å and 1.7±2.9 Fe at 3.57±0.20 Å for r2); therefore, they were constrained and optimized to 8 as the total number of Fe atoms. The resulting fit was marginally better than the fits obtained by constraining the combined Fe coordination numbers to 10, 12 and 16 (Fig. 5). The use of Ge, instead of Fe as the second metal shell at about 3.5-3.6 Å, was equally plausible when the fits were performed with the same set of parameters and constraints. This suggests that the amplitude and phase-shift functions of Ge and Fe are too close to distinguish the two types of backscattering waves by EXAFS. These local structural parameters are different than those reported by Pokrovsky et al. (2006) for a Ge-adsorbed goethite (i.e., 1 Ge at 3.30 Å) and an unknown co-precipitate with a Fe/Ge ratio of 3.6 (i.e., 1 Ge at 2.87 ± 0.04 Å and 2 Ge at 3.38 ± 0.02 Å).

Like the Ge K-edge EXAFS spectra, the Fe K-edge EXAFS spectra of the precipitates synthesized at different pH values from solutions with Fe/Ge molar ratios of 2 are identical (Fig. 6); therefore, they were averaged and presented as r2 (Fig. 7). Similarly, the spectra representing precipitates from solutions having a Fe/Ge molar ratio of 4 were averaged and presented as r4. The precipitate formed from the solution with a Fe/Ge molar ratio of 54 was presented as r54 and the precipitates formed from very dilute Ge solutions (i.e., Fe/Ge=105 and 213) were averaged and presented as r105+. The spectra representing the different synthesis concentrations display subtle differences at

high *k* but there is no trend or pattern as a function of the solution concentration. For instance, the r2 spectrum is more similar to that of the Ge-free six-line ferrihydrite (Fh6L) than to r4. If a trend existed, the r4 spectrum should have displayed more similarity to Fh6h.

EXAFS analysis of r2 indicates that the Fe–O radial distances are 1.96 ± 0.02 Å for 5.4 ± 1.4 oxygen atoms and 2.11 ± 0.02 Å for 0.6 oxygen atoms (Table 3). The asymmetric nature of the Fe-O bonding can be explained by the large variety of bonding environments that exist in the structure, such as Fe-O-Ge, Fe-O-Fe, Fe-OH-Fe and Fe-H_2O. Following the oxygen shell, 1.2 ± 0.3 and 2.1 ± 0.6 Fe atoms are detected at distances of 3.00 ± 0.02 and 3.43 ± 0.02 Å. The r4 spectrum is described by two oxygen shells having 3.8±0.6 and 2.2 oxygen atoms at 1.93 ± 0.02 Å and 2.06 ± 0.03 Å. The Fe shell as the next-nearest neighbours is split into 3 sub-shells at 2.93 ± 0.05, 3.04 ± 0.04 and 3.42 ± 0.01 Å with coordination numbers of 0.8 ± 0.5, 1.1 ± 0.4 and 1.7 ± 0.8. The short Fe-Fe distance is similar to the face-sharing Fe-Fe distance in hematite. The longer Fe-Fe distances are similar to those of r2 and are typical of edge-sharing and corner-sharing arrangements observed in Fe oxyhydroxides (Manceau and Drits 1993). The Fe-Fe distance of 3.42-3.43 Å is similar to the Ge-Fe distance (i.e., 3.38 ± 0.03 Å), and Fe and Ge have similar scattering amplitudes and phase shifts, suggesting that the detection of Fe-Ge pairs at this distance would be difficult at the Fe K-edge (see Supplementary materials). In essence, these measured local structural parameters of r2 and r4 are consistent with the classical ferrihydrite structure. The small spectral differences between r2 and r4 reflect changes imposed by the presence of Ge and other bonding constraints (Fig. 7).

EXAFS fitting of the spectra belonging to the dilute samples (r54 and r105+) also resulted in local structural parameters that are consistent with the classical ferrihydrite structure. The differences in the local structural parameters between the Ge-rich and dilute ferrihydrite precipitates are insignificant as they lie within the estimated uncertainty values.

DISCUSSION

Fitting of the Ge-EXAFS spectra indicated that Ge occurs as isolated tetrahedra surrounded by Fe atoms at nearly 3.38 Å and then by Fe or Ge atoms at nearly 3.54 Å distance for Ge-bearing ferrihydrites precipitated from both concentrated and dilute Ge solutions. These local structural parameters along with the similarity of the Ge-EXAFS spectra of the precipitates formed over a wide pH range from 2 to 13 imply that Ge is incorporated in the ferrihydrite structure. It appears based on the semi-quantitative TEM microanalyses that the incorporation is limited to about 17-20% of the total cations (Fe+Ge). The local structural data derived from Ge-EXAFS can also be explained by the adsorption of Ge onto very small ferrihydrite crystallites (i.e., 1-2 nm) and their aggregation aided by the highly-reactive surface Ge. However, there are no indications for the presence of subgrains within the ferrihydrite crystallites which measure about 5-6 nm. In addition, the uniformity of the ferrihydrite crystallite size and shape across the wide pH and compositional ranges, and the continuity of the lattice fringes across the particles would dictate against the occurrence of Ge as an adsorbed species.

In the new ferrihydrite structure (Fhyd6) of Michel et al. (2010), 20% of the total iron occurs in tetrahedral coordination. Maillot et al. (2011), Guyodo et al. (2011) and Peak and Regier (2012) claimed to have found evidences for the presence of 15 to 40% tetrahedral iron (^{IV}Fe) in ferrihydrite. We disagree with the EXAFS interpretation of Maillot et al. (2011) (20-30% ^{IV}Fe) because it suffers from unconstrained fitting of Fe-O pairs (Manceau 2011, Figs. S2 and S4 in the Supplementary materials).

As demonstrated in the Supplementary materials, the uncertainties in the determination of the Fe-O distances (i.e. ±0.01 Å) and the coordination numbers (i.e. 20% on each O shell) reported by Maillot et al. (2011) to calculate the amounts of ^{IV}Fe are overly optimistic. Our estimated minimum uncertainty levels associated with unconstrained fitting are ±0.02 Å for the Fe-O distances and 30% for the coordination numbers (Table S2). These uncertainties would be compounded by the experimental error, including statistical noise and systematic errors resulting from measurement and data reduction such as the shell-by-shell Fourier filtering. Uncertainties in the calculation of ^{IV}Fe would be 29-50% at best and as high as 52-116% (Fig.S4) suggesting that the amounts of ^{IV}Fe in ferrihydrite reported by Maillot et al. (2011) are not statistically different from those in maghemite (37.5%) and akaganeite (0%). Maillot et al. (2011)

also determined the average Fe-O distance by the Landweber iterative method of Rossberg and Funke (2010). This calculation is not convincing either because there is limited information with respect to the total number of iterations. In the Landweber approach, fit improvement is continuous, increasing with the number of iterations; however, there is a limit to the total number of iterations for producing statistically meaningful data, which requires an independent knowledge of the experimental errors associated with each data set. In summary, the fits performed by Maillot et al. (2011) at an extended *k*-range are inconclusive in terms of providing the needed finesses for determining the Fe-O distances in ferrihydrite in support of the tetrahedral Fe hypothesis.

In order to further elaborate on the claimed presence of 20 to 30% ^{IV}Fe in ferrihydrite, we compared the Fe-EXAFS spectra of nano- and micro-scale maghemite samples (Corrias et al. 2000) to our Ge-free Fh6L (Fig. 8a-h). First of all, Fourier transform magnitudes of the nano- and micro-sized maghemite clearly show that the Fe coordination numbers of the micro-scale maghemite are expectedly greater than those of the nano-scale counterpart while the oxygen coordination numbers remain unchanged, in agreement with the observations of Maillot et al. (2011). In addition, there are remarkable similarities between the long-range structures of the ferrihydrite with tetrahedral Fe (akdalaite model) and maghemite (Manceau 2011). Similarities also exist in the short-range structures as depicted by Michel et al. (2007; 2010). Furthermore, a reevaluation of the data presented by Maillot et al. (2011) indicates that the amount of ^{IV}Fe in ferrihydrite is not very different from that of maghemite (Supplementary materials). These observations rationalize the use of the Fe-EXAFS spectrum of nano-scale maghemite of Corrias et al. (2000) in our comparative evaluation. A clear shift to lower distances of the imaginary part corresponding to the oxygen shell is seen in the Fourier transform of maghemite relative to six-line ferrihydrite data, consistent with the presence of ^{IV}Fe in maghemite (Fig. 8f). The shift is present regardless of the integration range (i.e. k=2.3-14.2 Å^{-1} or 2.3-16.1 Å^{-1}). This is a definite point in that six-line ferrihydrite and maghemite have different Fe-O bonding environments and it argues strongly against the findings of Maillot et al. (2011) about the occupation of tetrahedral sites by Fe in ferrihydrite.

The other statement put forward by Maillot et al. (2011) from data fitting of the oxygen shell is that the detection of ^{IV}Fe would require EXAFS measurements at extended *k* ranges of 17 Å^{-1} and cryogenic temperatures. We tested this hypothesis by comparing our six-line ferrihydrite data recorded at room temperature to that of Manceau (2011) measured at liquid He temperature at *k* values of up to 16.1 Å^{-1} and 14.2 Å^{-1}. Figure 8b shows that the peak maximum of the Fe-O distribution is shifted to higher distances at low temperature, because the distribution of the Fe-O distances is wide and asymmetric, as discussed by Manceau (2011). At room temperature, this effect manifests itself by a broadening of the Fe-O peak of six-line ferrihydrite to higher *R* values relative to maghemite (Fig. 8f). Thus, the displacement of the Fe-O distance centroid to higher values at room temperature contradicts the need for low temperature measurements for the detection of ^{IV}Fe.

The argument of Peak and Regier (2012a) based on Fe L-edge XANES spectra is questionable as discussed in Manceau's (2012b) rebuttal because Peak and Regier (2012b) failed to acknowledge that the same spectral feature, interpreted as evidence for tetrahedral Fe, has been reported for cobalt and interpreted as a disorder effect (distribution of crystal field splitting). The claim of Guyodo et al. (2012) for the presence of tetrahedral iron in a synthetic six-line ferrihydrite sample based on X-ray magnetic circular dichroïsm measurements performed at Fe K- and L- edges is not convincing: firstly for the reasons outlined in the rebuttal papers by Manceau (2012b) and Hocking et al. (2012), and secondly because of the mistaken attribution of the antiferromagnetic properties to tetrahedral and octahedral Fe (Francombe and Rooksby 1959) instead of face-sharing Fe octahedra (Pernet et al. 1984; Drits et al. 1993b).

The ratio of octahedral Fe (^{VI}Fe) to tetrahedral Fe (^{IV}Fe) in the akdalaite model (i.e., ^{VI}Fe / ^{IV}Fe =4) would be analogous to our r2 and r4 samples with Fe/Ge≈4 if we assume that Ge substitutes for ^{IV}Fe, as proposed by Song et al. (2010). In this case, our Ge-EXAFS should produce data similar to the local structure around ^{IV}Fe in Fhyd6 and our Fe-O coordination numbers and distances should reflect only the octahedral Fe in Fhyd6. In Fhyd6, ^{IV}Fe is bonded to 10 ^{VI}Fe at about 3.38 Å, whereas our Ge-EXAFS spectra indicate that there are only six Fe atoms at that distance. On average, each ^{VI}Fe sees 7.5 ^{VI}Fe at distances between 2.91 and 3.49 Å. Based on the Fe-EXAFS of Ge-bearing

426 ferrihydrites, there are only 1 to 2 Fe at 2.93-3.04 Å and ~2 Fe at 3.42-3.43 Å, and this
427 accounts for less than half of the ^{VI}Fe of Fhyd6 in the 2.91-3.49 Å range. However, this
428 difference is marginal as it can be explained by disorder. The Ge-O distances (1.76 ± 0.01
429 Å) are much smaller than the ^{IV}Fe –O distances of Fhyd6 (1.91 ± 0.08 Å). A Ge for ^{IV}Fe
430 substitution would require the Ge-Fe distances to be shorter than the ^{IV}Fe-^{VI}Fe distances
431 of Fhyd6 because our Fe-O distances (1.98 ± 0.06 Å) are comparable, within the limits of
432 error, to the ^{VI}Fe-O distance (2.01 ± 0.08 Å) of Fhyd6. However, this is not the case. The
433 Ge-Fe distances of 3.38 ± 0.03 Å and 3.54 ± 0.08 Å are similar to the ^{IV}Fe-^{VI}Fe distances
434 of 3.38 ± 0.01 Å and 3.56 ± 0.07 Å of Fhyd6. In addition, our EXAFS data indicate that
435 the local structures of Ge and ^{VI}Fe do not change with increased Ge substitution, and this
436 casts serious doubts on the presence of ^{IV}Fe in the ferrihydrite structure. If ^{IV}Fe existed in
437 the ferrihydrite structure, then the measured Fe-O distances would have been longer in
438 the Ge-rich precipitates (r2 and r4) than those in the Ge-free Fh6L precipitate. The
439 similarity of the average Fe-O distances calculated from the data of Table 3, which are
440 1.98 Å for r2, 1.98 Å for r4 and 1.99 Å for Fh6L, does not support the presence of ^{IV}Fe in
441 the ferrihydrite structure. Furthermore, the similarity of the Fe-EXAFS spectra of r2, r4,
442 r105+ and Fh6L, representing the high, low and no Ge-bearing ferrihydrite precipitates,
443 indicates that the local structure of Fe is not affected by the presence of Ge. This
444 observation dictates against the presence of ^{IV}Fe.

445 The local structure of Ge can be conceptualized in the defect-free phase (i.e., "f-
446 phase") of the classical ferrihydrite structure through the use of a 2×2×1 supercell of the
447 f-phase (Fig. 9). The f-phase is composed of oxygens and hydroxyls closely-packed with
448 ABACA stacking and Fe randomly occupying 50% of the octahedral sites in each anion
449 layer (Drits et al. 1993a; Manceau 2009; 2011). Distribution of Fe across the anion layers
450 is such that there are no face-sharing arrangements between Fe octahedra along the B and
451 C planes of the structure and that hydroxyls are confined to the A and oxygen to the B
452 and C layers (Fig. 9a). The observed Fe-Fe distances of 3.00 to 3.04 Å in the Ge-bearing
453 ferrihydrite precipitates would correspond to the 2.96 Å distance of the f-phase
454 representing first nearest pairs of edge-sharing octahedra. In contrast, the 3.41-3.43 Å
455 distances correspond to the 3.30-3.50 Å distances representing the average of the second
456 nearest pairs of edge-sharing and the bridging or double corner-sharing octahedra. This

457 distribution partly explains why the effective coordination numbers for the second metal
458 shell reported in Table 2 are greatly reduced.

459 Using EXAFS-derived local structural data, Ge can be distributed in the f-phase
460 with the following constraints: (1) Ge occupies tetrahedral sites in the structure; (2) there
461 are no Ge-O-Ge linkages between the tetrahedra; and (3) no face-sharing between the Ge
462 tetrahedra and Fe octahedra is allowed. The resulting long-range configuration is of Ge
463 filling empty tetrahedral sites by occupying every other tetrahedral site along the *a* and *b*
464 directions in alternating octahedral layers (i.e., BA and CA or AB and AC layers of the
465 close-packing O/OH framework) (Fig. 9b,c). This corresponds to 25% occupancy of the
466 tetrahedral sites along the layers with Ge, or 12.5 % of the total tetrahedral sites. Three
467 adjacent octahedral sites in the same layer surrounding the tetrahedra must be vacant to
468 avoid face-sharing arrangement between the Ge tetrahedra and Fe octahedra which would
469 mean equal number of tetrahedra and octahedra in these layers. This results in a 75%
470 octahedral vacancy along the layers with Ge and 25% along the adjacent layers without
471 Ge (Fig. 10). Although this configuration differs from the 50% occupancy of each anion
472 layer in the f-phase, the bulk occupancy remains similar at 50%. The "apical oxygens" of
473 the tetrahedral sites are located along the B or C layers of the f-phase; therefore, the B
474 and C layers will have Ge-O-Fe and Fe-OH-Fe linkages with Fe-OH-Fe being three times
475 as many as the Ge-O-Fe linkages. The A layer, on the other hand, will have three times as
476 many Ge-O-Fe linkages as the Fe-OH-Fe linkages. The protons, confined to the A layers
477 in the Ge-free f-phase, will have to be redistributed in order to prevent Ge-OH-Fe
478 linkages because this O atom is already saturated, being bonded to three edge-sharing Fe
479 octahedra. Thus, in addition to reordering of the Fe occupancy, three-quarters of the OH
480 sites would have to move from the A to B and C layers. Like the Fe redistribution, this
481 does not change the bulk or average proportions of OH and O in the f-phase, and a
482 stoichiometry close to FeOOH is maintained in agreement with Hiemstra and Van
483 Riemsdijk (2009). In addition, each Fe octahedron contains three oxygens and three
484 hydroxyls, as for the Ge-free f-phase and all iron oxyhydroxides. With the incorporation
485 of Ge in the structure occupying 12.5% of the total tetrahedral sites and accompanying
486 redistribution of the Fe occupancy across the layers, Ge tetrahedra form 20% of the total

Ge+Fe cation sites, which is consistent with the constant Ge content of the r2 and r4 precipitates.

Occurrences or motifs of Ge in the BA+CA and AB+AC anion layers are identical within the limits of the symmetry elements (Fig. 9b,c). Rotating the supercell around the *c*-axis and flipping it across the *ab* plane is sufficient to demonstrate that the two motifs are indistinguishable. This is also confirmed by the close-packing notations as illustrated on Figure 11 with sequences that are equivalent through the lattice symmetry. The two motifs have the same XRD pattern and can co-exist in the same crystal. This means that it would be possible to maintain 50% Fe occupancy along individual layers as in the f-phase. In this case the mosaic Ge-Fe crystals would be short-range ordered, but long-range disordered with antiphase boundaries between the BA+CA and AB+AC Ge domains.

The local structure of Ge as illustrated on Figure 9 is such that a Ge tetrahedron is coordinated to 4 edge-sharing FeO_6 trimers or 12 FeO_6 octahedra through sharing of a common oxygen. This means that the local arrangement of ^{IV}Fe in Fhyd6 or the Keggin-like motif is possible in the f-phase of the classical ferrihydrite structure. The Fe1 octahedra of Fhyd6 (Fig. 9d, Michel et al. 2007) would then correspond to the octahedral layers defined by the AB and AC (Fig. 9b) or BA and CA (Fig. 9c) anion layers of the f-phase. It is possible that the flexibility of the f-phase in terms of accommodating tetrahedral ions with a Keggin-like motif may have contributed to some of the disagreements in the literature. What is needed is a justification for the coordination change from ^{VI}Fe to ^{IV}Fe during the hydrolysis of $Fe(H_2O)_6$ leading to the nucleation of ferrihydrite. The evidence suggests that Fe(III) is present in octahedral coordination in oxygenated ionic solutions and that initial polymerization of $Fe(O,OH)_6$ octahedra proceeds through the formation of dimers, trimers and tetramers (e.g., Bottero et al. 1994; Rose et al. 1997). In contrast, tetrahedral coordination of Fe(III), as observed in maghemite, appears to require the presence of organic compounds such as citric acid and/or Fe(II) in the starting solution.

In conclusion, the findings of the present study indicate that there is no compelling evidence for the presence of tetrahedrally coordinated iron in the ferrihydrite structure. Furthermore, the classical model does not require the transition of octahedrally

coordinated Fe in solution into a tetrahedral coordination in the ferrihydrite precipitate. Incorporation of Ge tetrahedra in the ferrihydrite structure is possible through the redistribution of octahedral Fe site occupancies and protonated oxygens in the f-phase. The flexibility of the classical ferrihydrite model in terms of accommodating a Keggin-like arrangement, possibly with two distinct orientations within the same crystal, allows tetrahedrally coordinated ions, such as Ge and possibly Si, to be incorporated in an octahedrally coordinated Fe structure. That is, there is no need to invoke Keggin-like clustering of tetrahedrally coordinated Fe in the akdalaite model of the ferrihydrite structure (e.g., Michel et al. 2010; Harrington et al. 2011; Xu et al. 2011) as the structure of Ge-free or Ge-bearing ferrihydrite can be readily rationalized using the existing f-phase.

ACKNOWLEDGEMENTS

The contributions of the following are acknowledged: Erika Revesz and Artis Huang, graduate students at the University of Ottawa for the synthesis work at CANMET, Fred Pearson of the Canadian Centre for Electron Microscopy of McMaster University for helping with the TEM characterization work, Derek Smith for powder XRD analyses, Robert Gordon of the PNC-CAT beamline of the Advanced Photon Source (APS) for helping with the EXAFS experiments. We thank Anna Corrias for sharing her maghemite spectra and Andre Rossberg for discussions on the Landweber iterations. The EXAFS measurements at APS were carried out under a General User Proposal to the senior author and a Partner User Proposal supported by the Natural Sciences and Engineering Research Council (NSERC) of Canada through a major facilities access grant. Research at the PNC-CAT beamline of APS, Argonne National Laboratory is supported by the US Department of Energy under Contracts W-31-109-Eng-38 (APS) and DE-FG03-97ER45628 (PNC-CAT). The study was funded in part by an NSERC Discovery Grant to the senior author and in part by Natural Resources Canada. We appreciate the critical comments received from three anonymous reviewers and the handling of the manuscript by the Associate Editor, Grant Henderson.

REFERENCES CITED

549 Ankudinov, A. L., Ravel, B., Rehr, J. J., and Conradson, S. D. (1998) Real space multiple
550 scattering calculation and interpretation of X-ray absorption near edge structure.
551 Physical Review, B 58, 7565.
552 Bottero, Y-V., Manceau, A., Villieras, F., and Tchoubar, D. (1994) Structure and
553 mechanism of formation of FeOOH(Cl) polymers. Langmuir, 10, 316-319.
554 Bull, C.L., McMillan, P.F., Itié, J-P., and Polian, A. (2004) X-ray absorption and EXAFS
555 studies of Ge coordination and bonding in high-pressure nitrides: b-Ge3N4
556 (phenacite) and g-Ge3N4 (spinel). Physica Status Solidi, A 201, 909–916.
557 Childs, C.W., Kanasaki, N., and Yoshinaga, N. (1982) Effect of heating in air on Si- and
558 Ge-containing ferrihydrites. Clay Science, 9, 65-80.
559 Corrias, A., Ennas, G., Mountjoy, G., and Paschina, G. (2000) An X-ray absorption
560 spectroscopy study of the Fe K edge in nanosized maghemite and in Fe_2O_3-SiO_2
561 nanocomposites. Physical Chemistry Chemical Physics, 2, 1045-1050.
562 Drewitt, J.W.E., Salmon, P.S., Barnes, A.C., Klotz, S., Fischer, H.E., and Crichton, W.A.
563 (2010) Structure of GeO_2 glass at pressures up to 8.6 GPa. Physical Review B, 81,
564 014202-1-13.
565 Drits, V.A., Sakharov, B.A., Salyn, A.L., and Manceau, A. (1993a) Structural model for
566 ferrihydrite. Clay Minerals, 28, 185–208.
567 Drits, V.A., Sakharov, B.A., and Manceau, A. (1993b) Structure of feroxyhite as
568 determined by simulation of X-ray diffraction curves. Clay Minerals, 28, 209–222.
569 Dyer, L., Fawell, P.D., Newman, O.M.G., and Richmond, W.R. (2010) Synthesis and
570 characterization of ferrihydrite/silica co-precipitates. Journal of Colloid and
571 Interface Science, 348, 65-70.
572 Eggleton, R.A. and Fitzpatrick, R.W. (1988) New data and a revised structural model for
573 ferrihydrite. Clays and Clay Minerals, 36, 111–124.
574 Francombe, M.H. and Rooksby, H.P. (1959) Structure transformations effected by the
575 dehydration of diaspore, goethite and delta ferric oxide. Clay Minerals Bulletin, 4,
576 1-14.
577 Guyodo, Y., Sainctavit, P., Arrio, M.-A., Carvallo, C., Lee Penn, R., Erbs, J. J., Forsberg,
578 B.S., Morin, G., Maillot, F., Lagroix, F., Bonville, P., Wilhelm, F., and Rogalev, A.

(2012) X-ray magnetic circular dichrosm provides strong evidence for tetrahedral iron in ferrihydrite. Geochemistry, Geophysics, Geosystems, 13, 1-9.

Harrington, R., Hausner, D.B., Xu, W., Bhandari, N., Michel, F.M., Brown, G.E.Jr., Strongin, D.R., and Parise, J.B. (2011) Neutron pair distribution function study of two-line ferrihydrite. Environmental Science and Technology, 45, 9883–9890.

Hattori, T., Nagai, T., Yamanaka, T., Werner, S., and Schulz, H. (2000) Single-crystal X-ray diffraction study of $FeGeO_3$ high-P clinopyroxene. American Mineralogist, 85, 1485-1491.

Hiemstra, T. and Van Riemsdijk, W.H. (2009) A surface structural model for ferrihydrite I: Sites related to primary charge, molar mass, and mass density. Geochimica et Cosmochimica Acta, 73, 4423-4436.

Hocking, R.K., Gates, W.P., and Cashion, J.D. (2012) Comment on "direct observation of tetrahedrally coordinated Fe(III) in ferrihydrite". Environmental Science and Technology, 46, 11471-11472.

Jambor, J.L. and Dutrizac, J.E. (1998) Occurrence and constitution of natural and synthetic ferrihydrite, a widespread iron oxyhydroxide. Chemical Reviews, 98, 2549–2586.

Janney, D.E., Cowley, J.M., and Buseck, P.R. (2000) Transmission electron microscopy of synthetic 2- and 6-line ferrihydrite. Clays and Clay Minerals, 48, 111-119.

Kato, von Katsuo, Takayama, E., and Kimizuka, N. (1983a) Eisen(II,III) germaniumoxid $Fe_{3,2}Ge_{1,8}O_8$. Acta Crystallographica, C39, 148-151.

Kato, von Katsuo, Takayama, E., Kimizuka, N., Haneda, H., and Yamamura, H. (1983b) Eisen(II,III) germaniumoxid $Fe_{15}Ge_8O_{36}$. Acta Crystallographica, C39, 151-154.

Li, X.F. and Liu, Y. (2010) First-principles study of Ge isotope fractionation during adsorption onto Fe(III)-oxyhydroxide surfaces. Chemical Geology, 278, 15-22.

Lu, K-Q, Zhao, Y-Q., and Chang, L-C. (1985) Local structure of Ge in binary oxide glasses by EXAFS. Chinese Physics Letters, 2, 113-116.

Maillot, F., Morin, G., Wang, Y., Bonnin, D., Ildefonse, P., Chaneac, C., and Calas, G. (2011). New insight into the structure of nanocrystalline ferrihydrite: EXAFS evidence for tetrahedrally coordinated iron(III). Geochimica et Cosmochimica Acta, 75, 2708-2720.

610 Manceau, A. (2009) Evaluation of the structural model for ferrihydrite derived from real-
611 space modeling of high-energy X-ray diffraction data. Clay Minerals, 44, 19–34.
612 _____ (2010) PDF analysis of ferrihydrite and the violation of Pauling's Principia.
613 Clay Minerals, 45, 225–228.
614 _____ (2011) Critical evaluation of the revised akdalaite model for ferrihydrite.
615 American Mineralogist, 96, 521–533.
616 _____(2012a) Critical evaluation of the revised akdalaite model for ferrihydrite—
617 Reply. American Mineralogist, 97, 255–256.
618 _____ (2012b) Comment on "direct observation of tetrahedrally coordinated Fe(III)
619 in ferrihydrite". Environmental Science and Technology, 46, 6882-6884.
620 Manceau, A. and Drits, V.A. (1993) Local structure of ferrihydrite and feroxyhite by
621 EXAFS spectroscopy. Clay Minerals, 28, 165-184.
622 Manceau, A., Lanson, M., and Geoffroy, N. (2007) Natural speciation of Ni, Zn, Ba, and
623 As in ferromanganese coatings on quartz using X-ray fluorescence, absorption, and
624 diffraction. Geochimica et Cosmochimica Acta, 71, 95–128.
625 Marchand, P. and Rancourt, D.G. (2009) General model for the aqueous precipitation of
626 rough-surface nanocrystals and application to ferrihydrite genesis. American
627 Mineralogist, 94, 1428–1439.
628 Martin, F., Ildefonse, P., Hazemann, J-L., Petit, S., Grauby, O., and Decarreau, A. (1996)
629 Random distribution of Ge and Si in synthetic talc: an EXAFS and FTIR study.
630 European Journal of Mineralogy, 8, 289-299.
631 Michel, F.M., Ehm, L., Antao, S.M., Lee, P.L., Chupas, P.J., Liu, G., Strongin, D.R.,
632 Schoonen, M.A.A., Phillips, B.L., and Parise, J.B. (2007) The structure of
633 ferrihydrite, a nanocrystalline material. Science, 316, 1726–1729.
634 Michel, F.M., Barrónc, V., Torrent, J., Morales, M.P., Serna, C.J., Boily, J.F., Liu, Q.,
635 Ambrosini, A., Cismasu, A.C., and Brown, G.E. Jr. (2010) Ordered ferrimagnetic
636 form of ferrihydrite reveals links among structure, composition, and magnetism.
637 Proceedings of the National Academy of Science, 107, 2787–2792.
638 Micoulaut, M., Cormier, L., and Henderson, G.S. (2006a) The structure of amorphous,
639 crystalline and liquid GeO_2. Journal of Physics: Condensed Matter, 18, R753–R784.

Micoulaut, M., Guissani, Y., and Guillot, B. (2006b) Simulated structural and thermal properties of glassy and liquid germania. Physical Reviews, E 73, 31504-1-11.

Peak, D. and Regier, T. (2012a) Direct observation of tetrahedrally coordinated Fe(III) in ferrihydrite. Environmental Science and Technology, 46, 3163-3168.

_____ (2012b) Response to comment on "Direct observation of tetrahedrally coordinated Fe(III) in ferrihydrite". Environmental Science and Technology, 46, 6885-6887.

Pernet, M., Obradors, X., Fontcuberta, J., Joubert, J.C., and Tejada, J. (1984) Magnetic structure and supermagnetic properties of δ-FeOOH. IEEE Transactions on Magnetics, MAG-20, 1524-1526.

Pokrovsky, O.S., Pokrovski, G.S., Schott, J., and Galy, A. (2006) Experimental study of germanium adsorption on goethite and germanium coprecipitation with iron hydroxide: X-ray absorption fine structure and macroscopic characterization. Geochimica et Cosmochimica Acta, 70, 3325-3341.

Price, D.L., Saboungi, M-L., and Barnes, A.C. (1998) Structure of vitreous germania. Physical Review Letters, 81, 3207-3210.

Rancourt, D.G. and Meunier, J.F. (2008) Constraints on structural models of ferrihydrite as a nanocrystalline material. American Mineralogist, 93, 1412–1417.

Ravel, B. and Newville, M. (2005) ATHENA, ARTEMIS, HEPHAESTUS: data analysis for X-ray absorption spectroscopy using IFEFFIT. Journal of Synchrotron Radiation, 12, 537–541.

Rose, J., Manceau, A., Masion, A., and Bottero, Y-V. (1997) Structure and mechanism of formation of $FeOOH(NO_3)$ oligomers in the early stages of hydrolysis. Langmuir, 13, 3240-3246.

Rossberg, A. and Funke H. (2010) Determining the radial pair distribution function from X-ray absorption spectra by use of the Landweber iteration method. Journal of Synchrotron Radiation, 17, 280-288.

Saleh, A.M. and Jones, A.A. (1984) The crystallinity and surface characteristics of synthetic ferrihydrite. Clay Minerals, 19, 745–755.

669 Song, Y., Bac, B.H., Lee, Y-B., Kim, M.H., Yoon, W-S, Kim, J.H., and Moon, H-S.
670 (2010) Ge-incorporation into 6-line ferrihydrite nanocrystals. Cryst. Eng. Comm.,
671 12, 1997-2000.
672 Welch, M.D., Cooper, M.A., and Hawthorne, F.C. (2001) The crystal structure of
673 brunogeierite, Fe_2GeO_4 spinel. Mineralogical Magazine, 65, 441-444.
674 Xu, W., Hausner, D.B., Harrington, R., Lee, P.L., Strongin, D.R., and Parise, J.B. (2011)
675 Structural water in ferrihydrite and constraints this provides on possible structure
676 models. American Mineralogist, 96, 513–520.
677

678 **FIGURE CAPTIONS**

679 **FIGURE 1**. XRD patterns of the precipitates made from solutions having various Fe/Ge
680 molar ratios. Italic numbers above the patterns are *d*-spacings in Å. Corresponding *hkl*
681 reflections of ferrihydrite (f-phase) are given in parentheses. Small peaks at ~21° in the
682 precipitates with Fe/Ge ratios of 4 (pH13), 71, 105, 213 and 435 are indicative of the
683 presence of minor goethite.
684 **FIGURE 2**. TEM photomicrographs showing equant and platy ferrihydrite crystallites.
685 Top left: r2 pH 5; top right: r2 pH 10; bottom left: r4 pH 5; bottom right: r4 pH 10.
686 **FIGURE 3**. HRTEM photomicrographs of ferrihydrite crystallites with rounded to
687 hexagonal outlines and showing well-developed lattice fringes. Top left: r2 pH 10; top
688 right: r2 pH 13; bottom left: r4 pH 2; bottom right: r4 pH 10.
689 **FIGURE 4**. k^3-weighted Ge K-edge EXAFS spectra of the precipitates. Spectra
690 identified by the Fe/Ge molar ratio (number preceding dash) and synthesis pH (number
691 following dash).
692 **FIGURE 5.** k^3-weighted Ge K-edge EXAFS spectra and their Fourier transforms.
693 Experimental spectra shown in black solid lines and simulations in red circle lines.
694 **FIGURE 6.** k^3-weighted Fe K-edge EXAFS spectra of the precipitates. Spectra
695 identified by the Fe/Ge molar ratio (number preceding dash) and synthesis pH (number
696 following dash).
697 **FIGURE 7.** k^3-weighted Fe K-edge EXAFS spectra and their Fourier transforms.
698 Experimental spectra shown in black solid lines and simulations in red circle lines.

FIGURE 8. Comparison of k^3-weighted Fe K-edge EXAFS spectra of ferrihydrite and maghemite and their Fourier transforms superimposed with imaginary parts. (a and b) six-line ferrihydrite at room (black) vs. liquid He (blue) temperatures; (c and d) nano- (red) vs. micro-sized (purple) maghemite; (e and f) six-line ferrihydrite at room temperature vs. nano-sized maghemite with integrations to *k* values of 16.1 (black and red); (g and h) six-line ferrihydrite at liquid He (blue) temperature vs. nano-sized maghemite (red). Six-line ferrihydrite spectrum collected at liquid He temperatures are from Manceau (2011) and maghemite spectra from Corrias et al. (2000). The y-scales are identical for all spectra and Fourier transforms.

FIGURE 9. Polyhedral representation of ferrihydrite (f-phase) using a 2×2×1 supercell with 50% Fe (brown) occupancy (a) and with Ge tetrahedra (violet) occupying 25% of tetrahedral sites in the BA and CA anion layers (b) or the AB and AC layers (c). Total tetrahedral site occupancy of the supercell is 12.5%. Note the changes in Fe occupancy and O (red) and OH (grey) distribution among the anion layers due to Ge incorporation. With Ge corner-linked to four edge-sharing FeO_6 trimers, the f-phase possesses Keggin-like clusters in two different orientations (b and c), that are symmetrically equivalent. Also shown is the unit cell of the Fhyd6 structure (d) for its similarity to the f-phase with Ge occurring along BA and CA layers (b). Fhyd6 structure (Fe1: light brown; Fe2: pink; Fe3: yellow) is based on Michel et al. (2007).

FIGURE 10. Polyhedral representation of Ge (violet) occupying tetrahedral sites along the BA and CA layers of ferrihydrite (f-phase).

FIGURE 11. Sketch of atomic positions in a 2×2×1 supercell of the f-phase demonstrating the identical nature of the two motifs arising from the incorporation of Ge in BA+CA and AB+AC anion layers with close-packing notations. Fe: light brown; Ge: violet; O/OH: red.

TABLE 1. Particle sizes of the precipitates formed from solutions with Fe/Ge molar ratios of 2 and 4

Sample number	Solution Fe/Ge	pH	Particle size (nm)				
			average	StDv	min	max	n
2-r2	2	2	5.2	1.0	3.1	8.3	96
5-r2	2	5	5.5	1.0	3.1	8.1	135
10-r2	2	10	5.6	1.1	2.3	8.4	128
13-r2	2	13	6.2	1.3	2.6	8.7	91
2-r4	4	2	6.2	1.6	2.9	12.2	141
5-r4	4	5	5.7	1.2	2.3	8.7	177
10-r4	4	10	6.0	1.5	2.9	10.5	86
13b-r4	4	13	6.7	1.7	3.6	11.3	97
13t-r4	4	13	5.8	1.6	2.6	10.9	127

Fe/Ge is molar ratio; StDv: standard deviation; min: minimum; max: maximum; n: number of particles measured

TABLE 2. Local structural parameters determined from Ge-EXAFS

		N	*R*	σ^2	$\Delta E0$	*rf*	rX^2
r2	O	4.8±0.4	1.76±0.00	0.0043	1.0	0.0078	768
	MS21	12*	3.16±0.05	0.0023			
	Fe1	6.3±1.4	3.38±0.03	0.0109			
	Fe2	1.7[c]	3.54±0.08	"			
r4	O	4.8±0.3	1.77±0.00	0.0042	1.6	0.0065	487
	MS21	12*	3.15±0.04	0.0020			
	Fe1	6.0±1.1	3.38±0.02	0.0102			
	Fe2	2.0[c]	3.54±0.06	"			
r43+	O	4.8±0.4	1.76±0.00	0.0031	2.3	0.0080	29
	MS21	12*	3.14±0.05	0.0013			
	Fe1	6.2±0.8	3.38±0.01	0.0090			
	Fe2	1.8[c]	3.56±0.05	"			

Fit performed in *R*-space (*R*=1-3.5; *k*=3-15 $Å^{-1}$); amplitude reduction factor (S_0^2) is constrained to 0.9; *N*: coordination number; *R*: interatomic distance (Å); σ^2: Debye–Waller parameter ($Å^2$); $\Delta E0$: energy offset (eV); *rf*: r-factor and rX^2 reduced chi square as the goodness-of-fit parameters; Multiple scattering path, MS21 refers to Ge–O1–O2; * Fixed value; [c] constrained to 8 as total Fe; Debye-Waller parameters of Fe2 were constrained to be identical with Fe1.

TABLE 3. Local structural parameters determined from Fe-EXAFS

		N	*R*	σ^2	$\Delta E0$	*rf*	rX^2
r2	**O1**	**5.4±1.4**	**1.96±0.02**	**0.0103**	**-3.1**	**0.0118**	**751**
	O2	**0.6[c]**	**2.11±0.02**	**"**			
	Fe1	**1.2±0.3**	**3.00±0.02**	**0.0077**			
	Fe2	**2.1±0.6**	**3.43±0.02**	**"**			
r4	**O1**	**3.8±0.6**	**1.93±0.02**	**0.0077**	**-2.9**	**0.0103**	**439**
	O2	**2.2[c]**	**2.06±0.03**	**"**			
	Fe1	**0.8±0.5**	**2.93±0.05**	**0.0065**			
	Fe2	**1.1±0.4**	**3.04±0.04**	**"**			
	Fe3	**1.7±0.8**	**3.42±0.01**	**"**			
r54	**O1**	**4.1±0.9**	**1.95±0.03**	**0.0085**	**-1.8**	**0.0107**	**252**
	O2	**1.9[c]**	**2.08±0.05**	**"**			
	Fe1	**1.6±1.4**	**3.03±0.03**	**0.0096**			
	Fe2	**1.7±1.4**	**3.41±0.03**	**"**			
r105+	**O1**	**5.4±0.9**	**1.98±0.02**	**0.0105**	**-1.2**	**0.0108**	**488**
	O2	**0.6[c]**	**2.16±0.10**	**"**			
	Fe1	**1.5±0.7**	**3.03±0.02**	**0.0076**			
	Fe2	**1.1±0.5**	**3.43±0.02**	**"**			
Fh6L	**O1**	**3.4±0.9**	**1.92±0.03**	**0.0073**	**-2.7**	**0.0128**	**1054**
	O2	**2.6[c]**	**2.05±0.04**	**"**			
	Fe1	**2.5±2.9**	**3.04±0.04**	**0.0129**			
	Fe2	**3.4±3.9**	**3.43±0.03**	**"**			

Fit performed in *R*-space (*R*=1.1-3.8 Å; *k*=2.5-15 $Å^{-1}$ for r2 and r4; *k*=3-13 $Å^{-1}$ for r54, r105+ and Fh6L); amplitude reduction factor (S_0^2) is constrained to 0.8; *N*: coordination number; *R*: interatomic distance (Å); σ^2: Debye–Waller parameter ($Å^2$); $\Delta E0$: energy offset (eV); *rf*: r-factor and rX^2 reduced chi square as the goodness-of-fit parameters; * Fixed value; [c] constrained to 6 as total O; Debye-Waller parameters of subsequent O and Fe shells were constrained to be identical with the initial shell values.

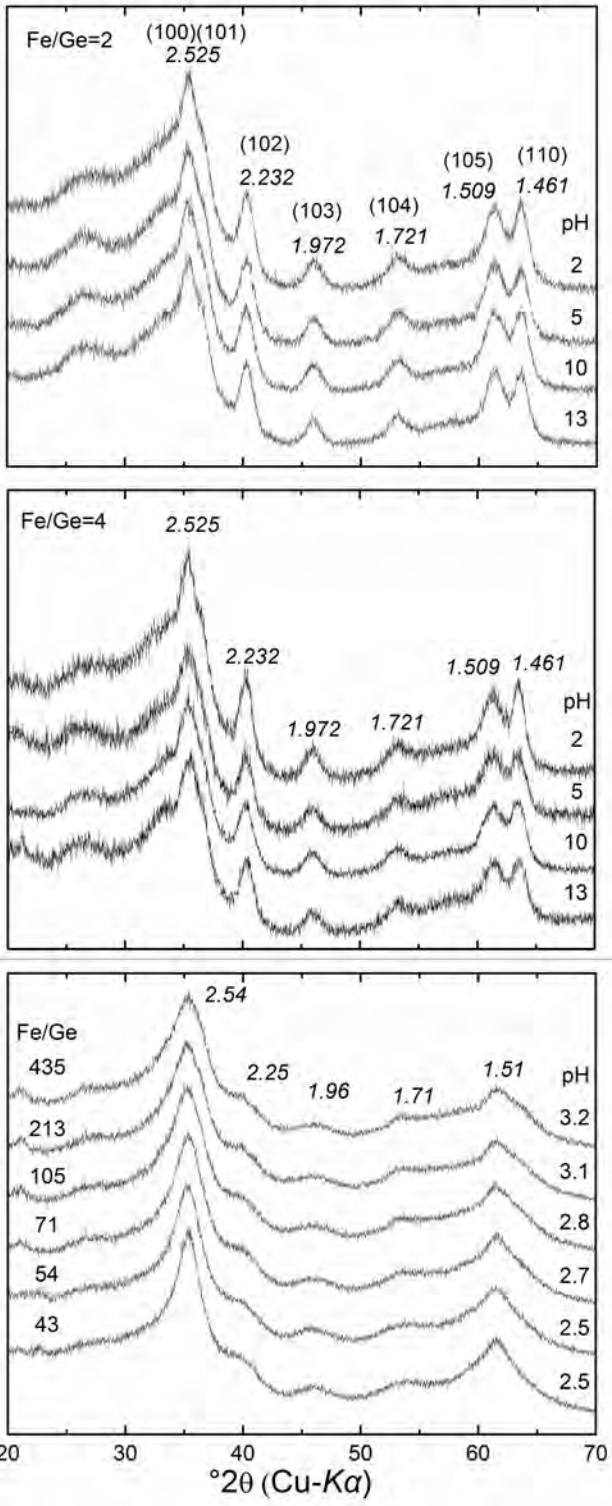
Fe/Ge=2
(100)(101)
2.525
(102)
2.232
(103)
1.972
(104)
1.721
(105)
1.509
(110)
1.461
pH
2
5
10
13
Fe/Ge=4
2.525
2.232
1.972
1.721
1.509
1.461
pH
2
5
10
13
Fe/Ge
435
213
105
71
54
43
2.54
2.25
1.96
1.71
1.51
pH
3.2
3.1
2.8
2.7
2.5
2.5
20
30
40
50
60
70
°2θ (Cu-Kα)

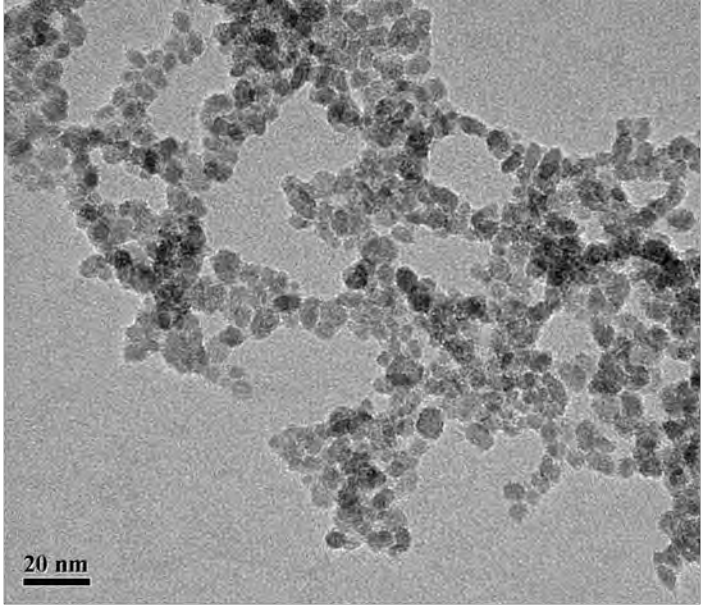
20 nm

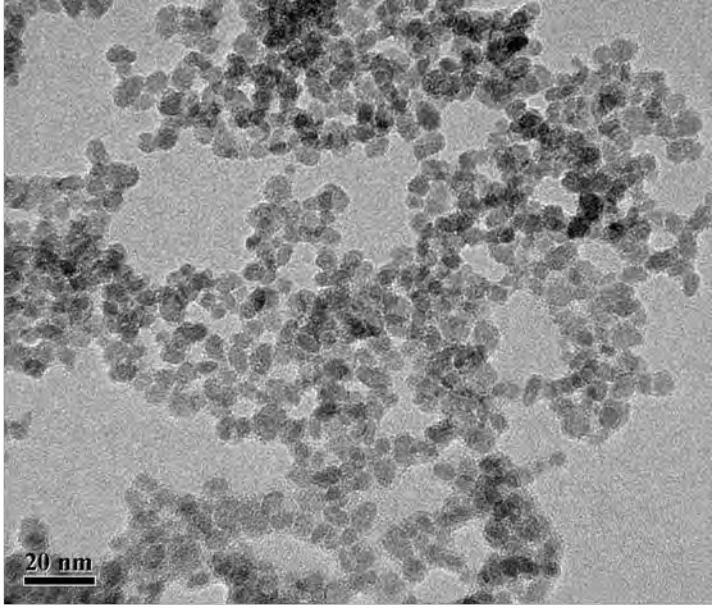
20 nm

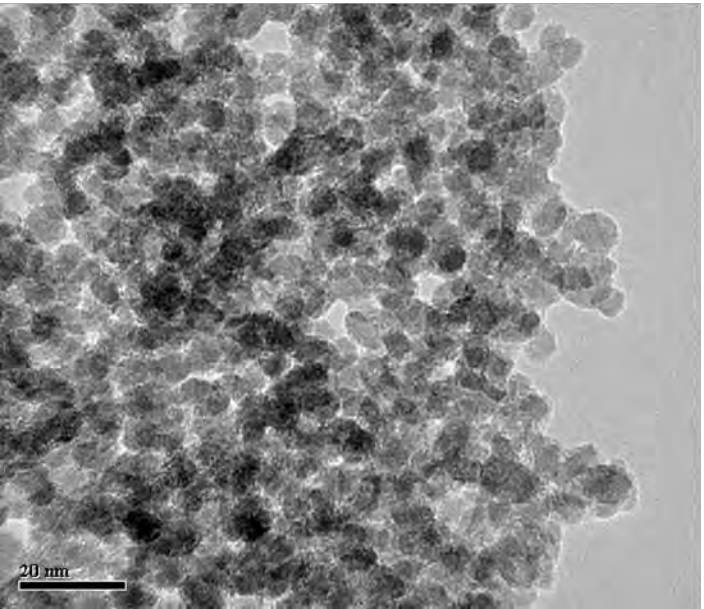
20 nm

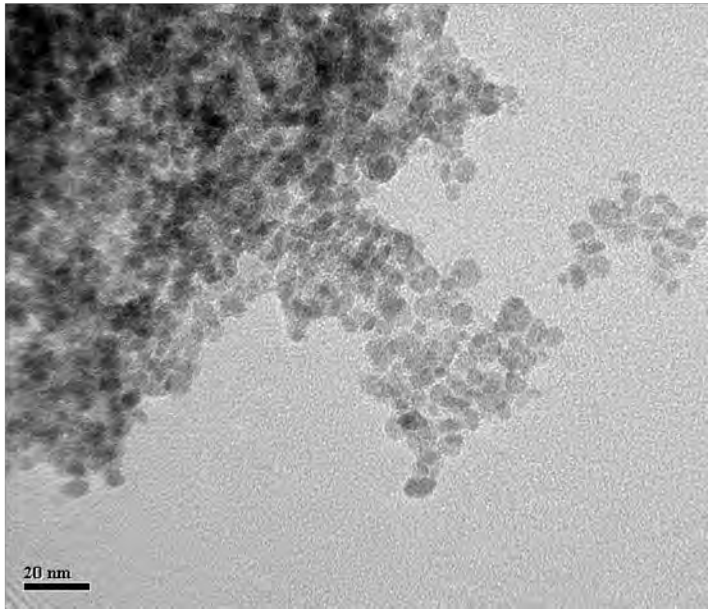
20 nm

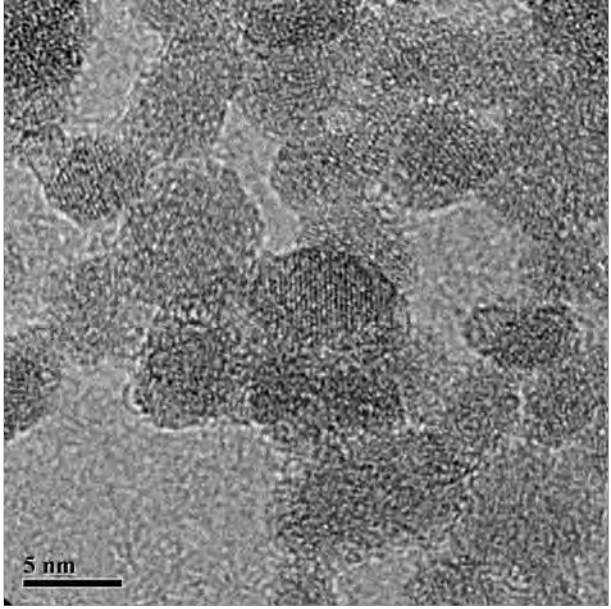
5 nm

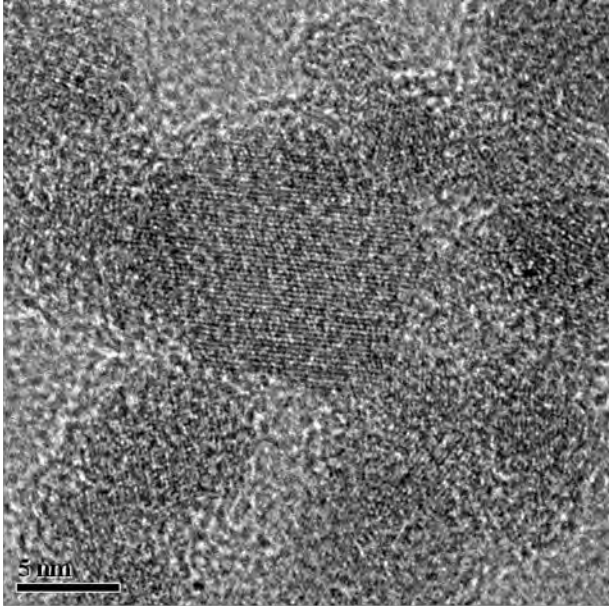
5 nm

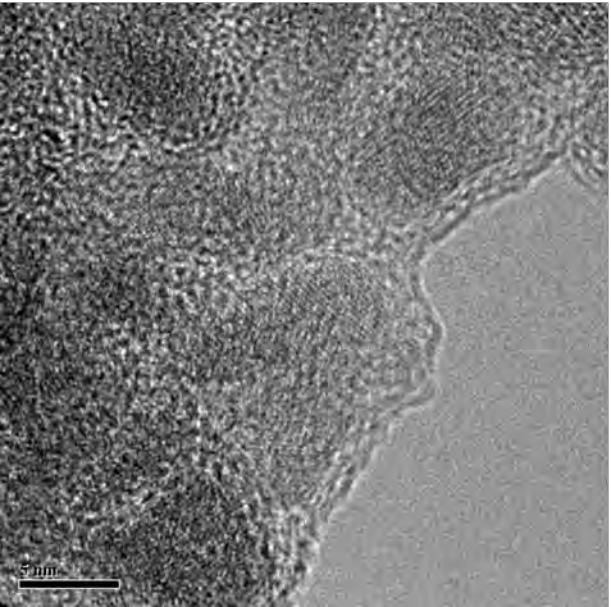
5 nm

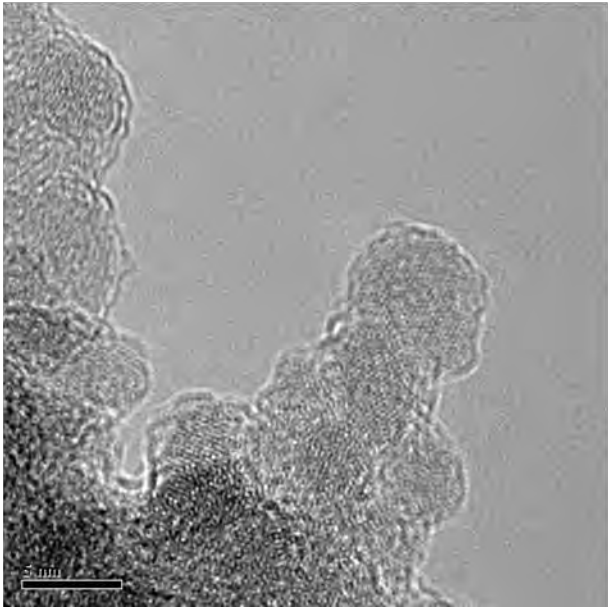
5 nm

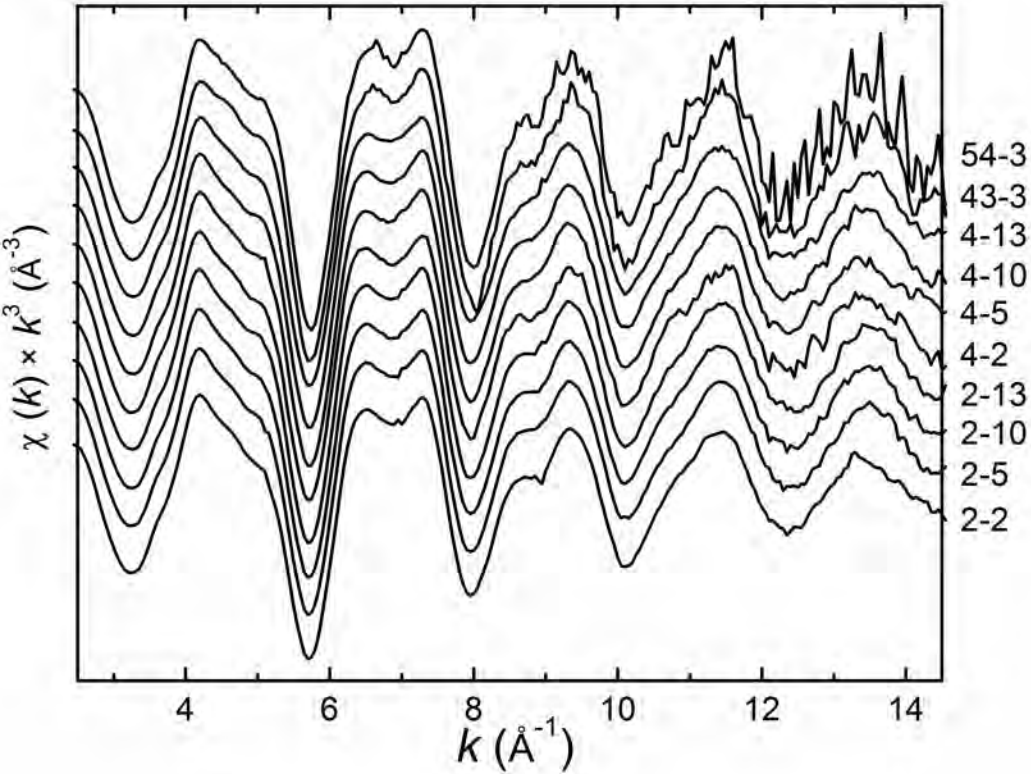
54-3
43-3
4-13
4-10
4-5
4-2
2-13
2-10
2-5
2-2
χ (k) × k3 (Å-3)
4
6
8
10
12
14
k (Å-1)

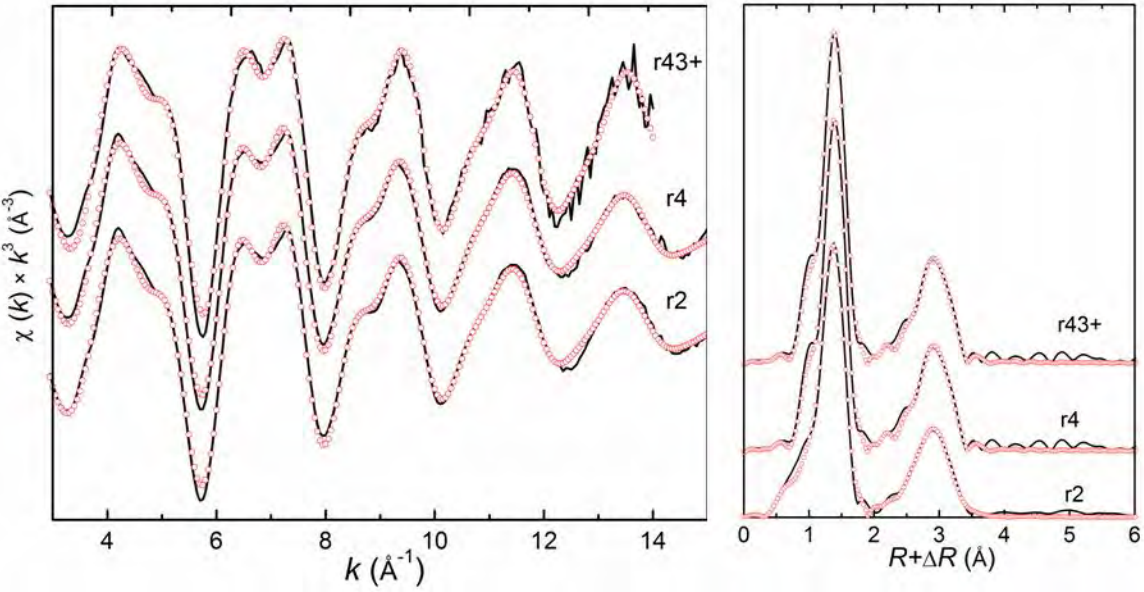
r43+
r4
r2
χ (k) × k³ (Å⁻³)
k (Å⁻¹)
4
6
8
10
12
14
r43+
r4
r2
R+ΔR (Å)
0
1
2
3
4
5
6

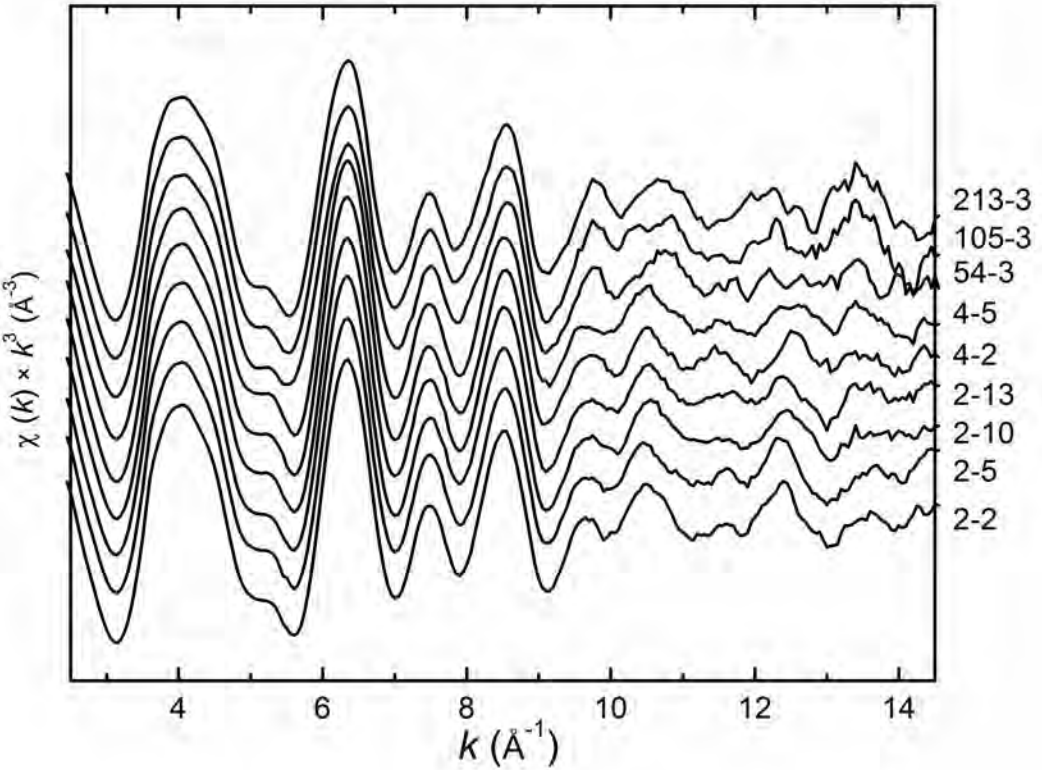
213-3
105-3
54-3
4-5
4-2
2-13
2-10
2-5
2-2
χ (k) × k³ (Å⁻³)
4
6
8
10
12
14
k (Å⁻¹)

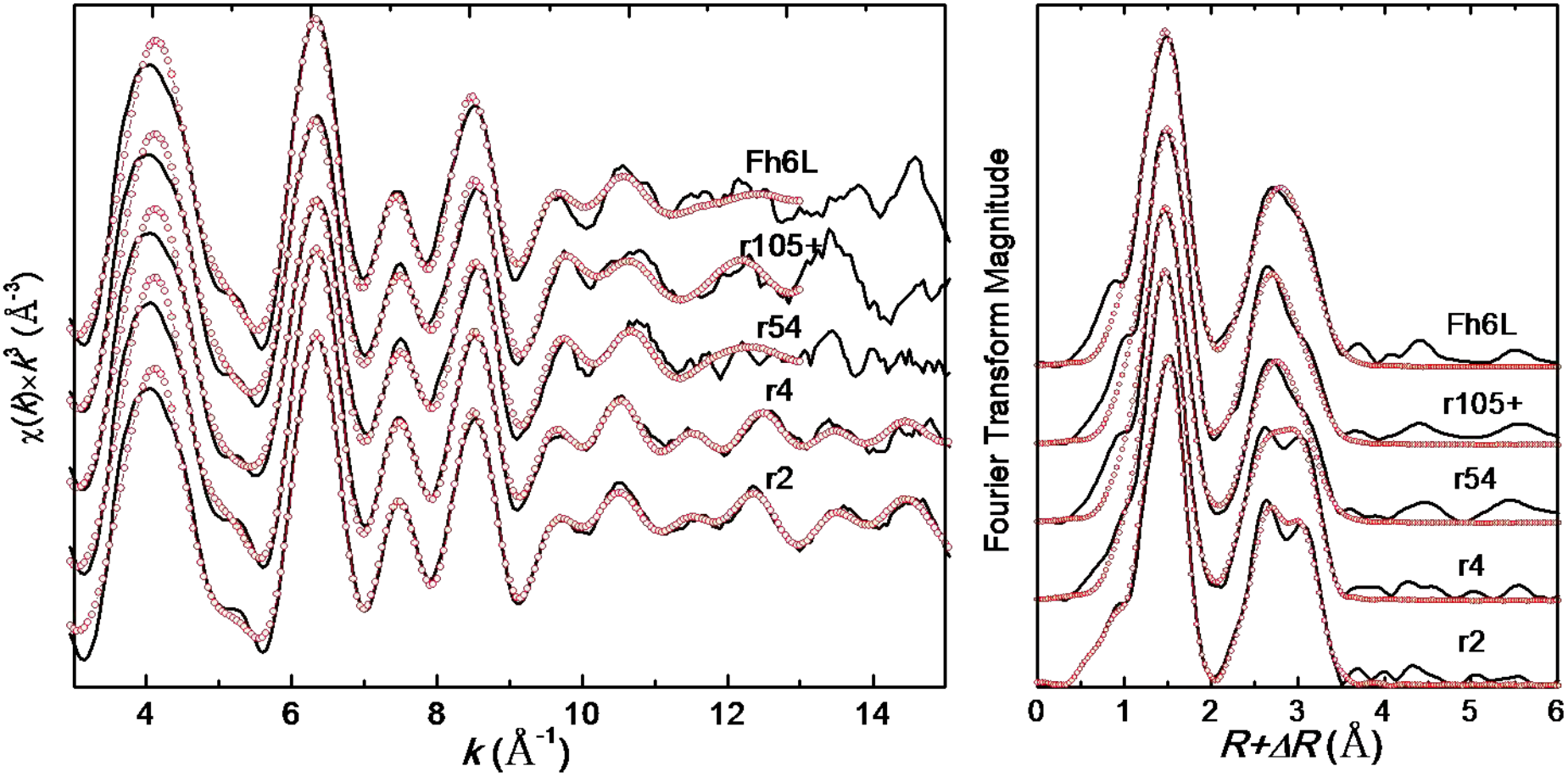
Fh6L
r105+
r54
r4
r2
χ(k)×k³ (Å⁻³)
k (Å⁻¹)
4
6
8
10
12
14
Fourier Transform Magnitude
R+ΔR (Å)
0
1
2
3
4
5
6

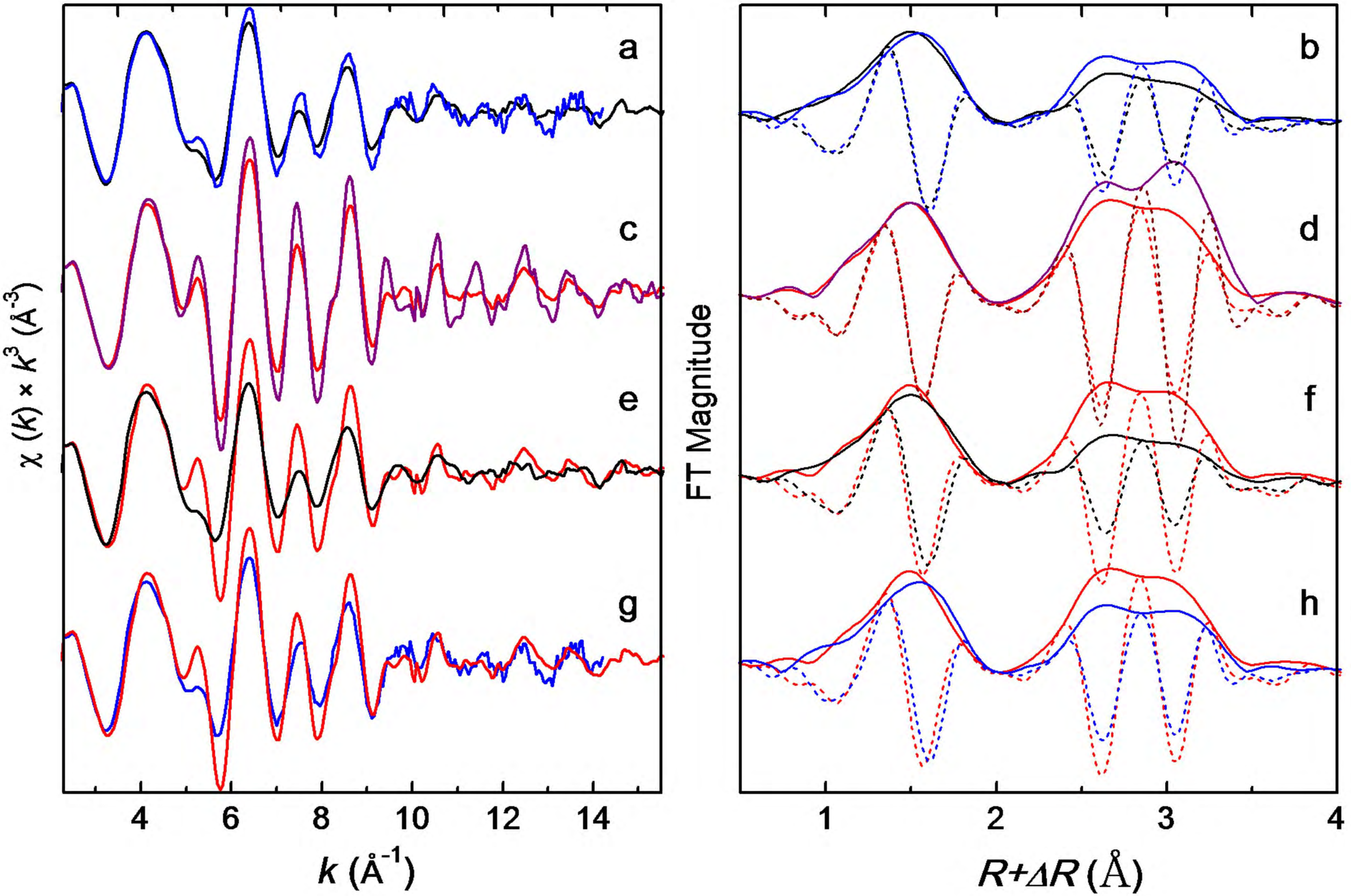
a
b
c
d
e
f
g
h
χ (k) × k³ (Å⁻³)
FT Magnitude
4
6
8
10
12
14
k (Å⁻¹)
1
2
3
4
R+ΔR (Å)

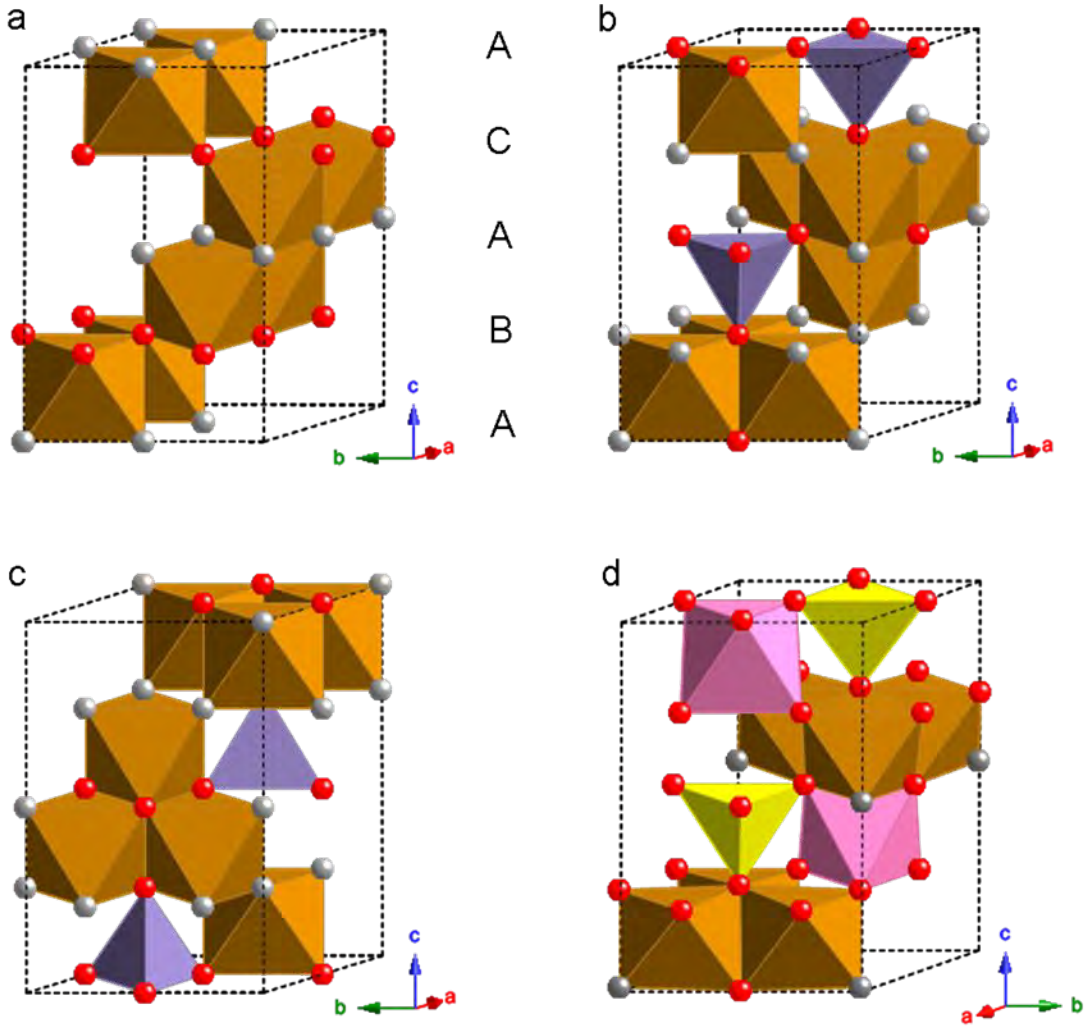
a
A
C
A
B
A
b
c
d
c
b
a

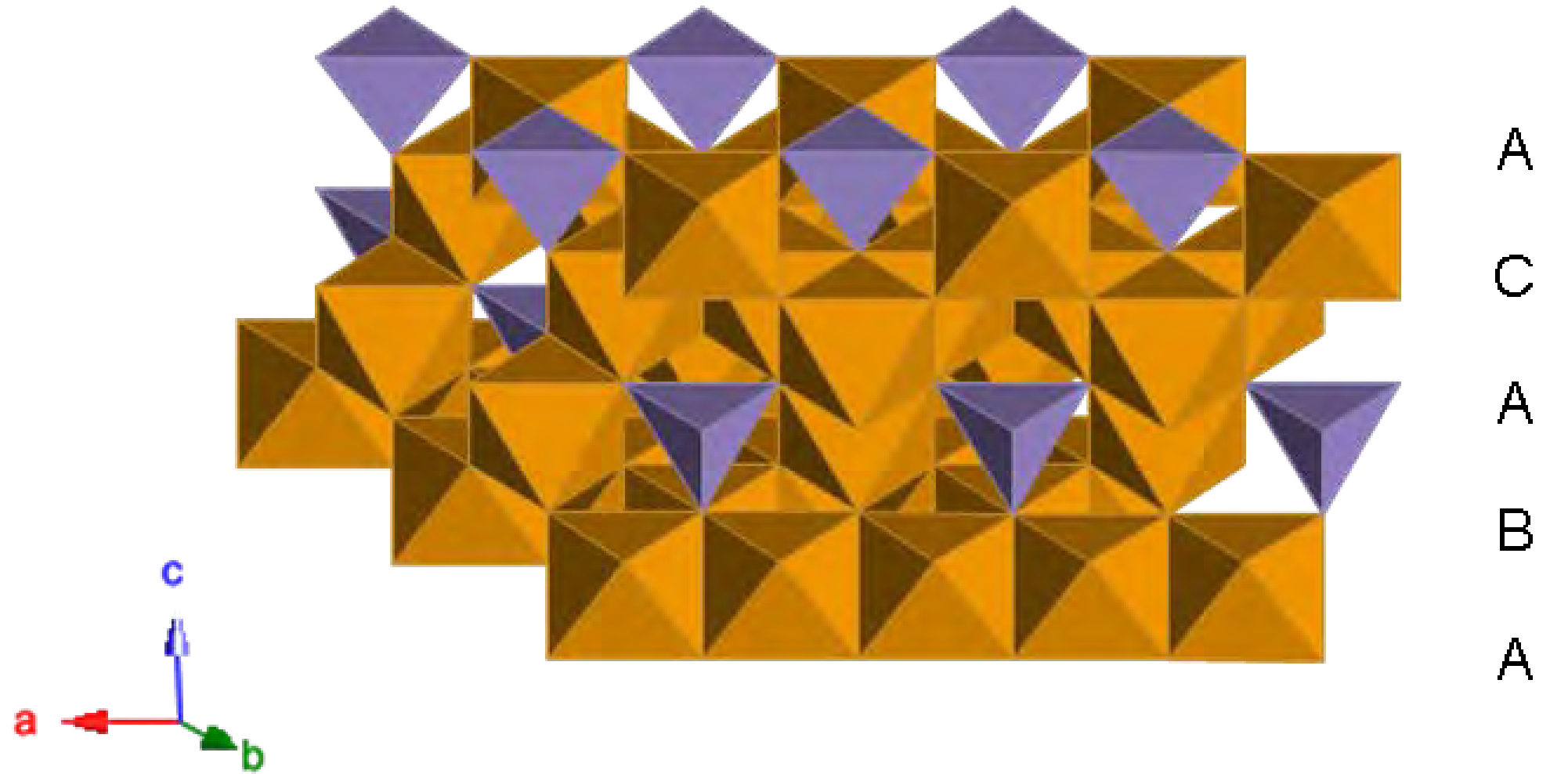
A
C
A
B
A
c
a
b

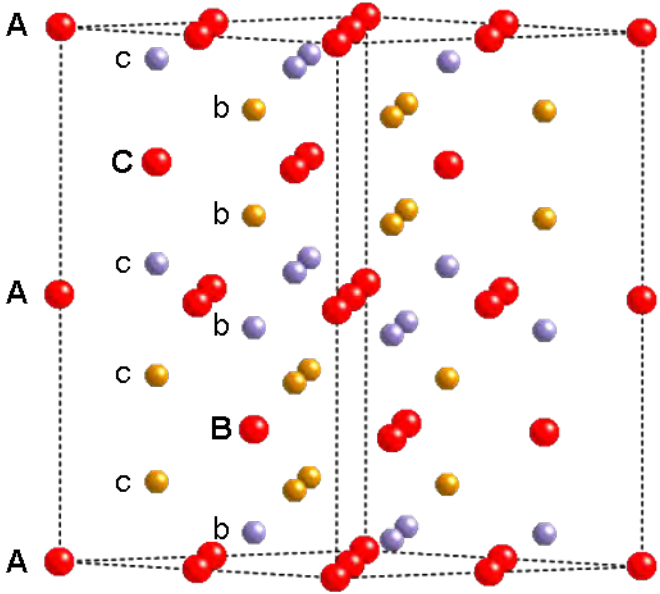
A
c
b
C
b
c
A
b
c
B
c
b
A

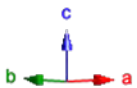
c
b
a

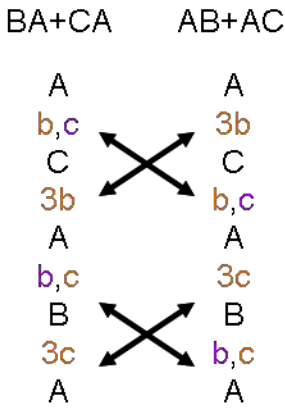
BA+CA
AB+AC
A
b,c
C
3b
A
b,c
B
3c
A
A
3b
C
b,c
A
3c
B
b,c
A